

Experimental Studies

Christoph Bremer, MD
Mona Mustafa, MD
Alex Bogdanov, Jr, PhD
Vasilis Ntziachristos, PhD
Alexander Petrovsky, MD
Ralph Weissleder, MD, PhD

Index terms:

Angiogenesis
Contrast media, experimental studies
Experimental study
Neoplasms, experimental studies
Neoplasms, radionuclide studies

Published online before print

10.1148/radiol.2261012140

Radiology 2003; 226:214–220

Abbreviations:

LCDIO = long-circulating
dextrinated iron oxide
VEGF = vascular endothelial growth
factor
VVF = vascular volume fraction

¹ From the Center for Molecular Imaging Research, Massachusetts General Hospital and Harvard Medical School, Bldg 149, 13th St, 5406, Charlestown, MA 02129. Received January 9, 2002; revision requested February 4; revision received April 2; accepted May 23. Address correspondence to R.W. (e-mail: weissleder@helix.mgh.harvard.edu).

Author contributions:

Guarantor of integrity of entire study, R.W.; study concepts, C.B., R.W.; study design, A.B., C.B., R.W.; literature research, M.M., C.B., R.W.; experimental studies, V.N., C.B.; data acquisition, A.P., V.N., C.B.; data analysis/interpretation, V.N., M.M., C.B., R.W.; statistical analysis, C.B.; manuscript preparation, C.B., R.W.; manuscript definition of intellectual content, R.W.; manuscript editing, C.B., R.W.; manuscript revision/review and final version approval, R.W.

© RSNA, 2002

Steady-State Blood Volume Measurements in Experimental Tumors with Different Angiogenic Burdens—A Study in Mice¹

PURPOSE: To experimentally validate the effectiveness of magnetic resonance (MR) imaging enhanced with long-circulating iron oxide for measurement of vascular volume fractions (VVF) as indicators of angiogenesis in different experimental tumor models.

MATERIALS AND METHODS: Tumors with differing degrees of angiogenesis—9L rodent gliosarcoma, DU4475 human mammary adenocarcinoma, HT1080 human fibrosarcoma, and EOMA hemangioendothelioma—were implanted in nude mice. Tumoral VVFs were measured at submillimeter voxel resolutions by using 1.5-T MR imaging. A technetium-labeled intravascular radiotracer was injected into a subset of the animals to validate the MR imaging measurements. Microvessel density and vascular endothelial growth factor (VEGF) also were measured. Statistical analysis was performed with analysis of variance.

RESULTS: High-resolution multisection MR maps of tumor blood volume were obtained in all tumor models. Mean tumoral VVF differed significantly among the different tumors: $2.1\% \pm 0.3$ (standard error of mean) for 9L gliosarcoma, $3.1\% \pm 0.4$ for DU4475 mammary adenocarcinoma, $5.5\% \pm 0.8$ for HT1080 fibrosarcoma, and $6.6\% \pm 0.9$ for EOMA hemangioendothelioma ($P < .01$). There was a strong correlation between the MR imaging and radiotracer measurements. There was considerable intra- and intertumoral heterogeneity among the VVFs. MR imaging measurements were in accordance with conventional measurements of angiogenesis, such as microvessel density count and VEGF.

CONCLUSION: Measurements of tumoral VVF at high-resolution MR imaging with long-circulating iron oxide are feasible and correlate with angiogenic burden in experimental tumor models.

© RSNA, 2002

Angiogenesis is broadly defined as the formation of new blood vessels from preexisting vasculature. Angiogenesis occurs physiologically—for example, during embryonic development and wound healing. In adults, the normal vascular network is usually quiescent and regulated by tightly controlled angiogenesis inducers and inhibitors. In certain pathologic conditions, this balance is shifted and the result is chaotic capillary growth. Up-regulation and/or down-regulation of the angiogenic process is an important feature of approximately 30 diseases, including cancer, cardiovascular disease, immunologic disease, and diabetes. The molecular basis of angiogenic control is slowly being recognized (1–4), and an ever-increasing number of angiogenesis inhibitors (eg, for tumor treatment) and promoters (eg, for ischemia treatment) are becoming the subject of clinical trials.

The continued development of newer and more efficient angiogenesis inhibitors (5) has prompted the need to develop and validate imaging techniques to measure the physiologic and molecular surrogate markers of angiogenesis. In particular, imaging measurement techniques that are sensitive to tumoral microvessels (ie, vessels $< 20 \mu\text{m}$ in

diameter) and yield high spatial resolution for depiction of “hotbeds” of angiogenesis (ie, areas of extensive new vessel growth) are desirable. Because the tumors and metastases in patients involved in clinical trials are often multifocal and large (ie, end stage), such imaging techniques should also be capable of complete tumor coverage rather than limited single-section measurements. Rapid-sequence, single-section imaging measurements performed with low-molecular-weight contrast agents have been used to extract first-pass kinetics and derive mathematical parameters (6–10). Reliable multisection, steady-state, high-resolution imaging, however, requires the use of a blood-pool contrast agent—that is, one with which a constant concentration of the agent stays within the intravascular space during the entire time of imaging. Although a number of such agents have been used in experimental studies (11,12), few are likely to be developed for clinical use.

One of the few classes of clinically viable, truly intravascular imaging agents that are being developed for clinical use are the long-circulating dextrinated iron oxide (LCDIO) preparations for use with magnetic resonance (MR) imaging (13,14). Before these agents are adapted for use in imaging tumor vascularity, however, their effectiveness must be experimentally validated. Thus, a model LCDIO preparation that has a blood half-life of several hours *in vivo* and is similar to preparations used in clinical trials (15) needs to be tested. Therefore, the purpose of our study was to experimentally validate the effectiveness of MR imaging performed with LCDIOs in the measurement of vascular volume fractions (VVF) as indicators of tumor angiogenesis in different experimental tumor models.

MATERIALS AND METHODS

Tumor Models and Cell Culture

A number of different human and murine tumor models were initially screened to determine their degree of vascularization (ie, angiogenic burden). Four specific tumor models were chosen because of the spectrum of microvessel density counts in these cancers observed clinically. Three of the primary cell lines used in this study were obtained from the American Tissue Culture Collection, Manassas, Va: 9L, a rodent gliosarcoma; HT1080, a human fibrosarcoma; and DU4475, a human breast cancer. The fourth cell line, EOMA, is a hemangioen-

dothelioma-derived cell line that was provided by Obeso et al (16).

The 9L and EOMA cells were cultured in modified Eagle's medium (Cellgro; Mediatech, Washington, DC) supplemented with 2 mmol/L of L-glutamine and Earle salt solution with 1.5 g/L of sodium bicarbonate and 10% heat-inactivated fetal bovine serum (Cellgro FBS; Mediatech) at 37°C in a humidified 5% CO₂ atmosphere. The HT1080 cells were cultured in the same medium supplemented with 0.1 mmol/L of nonessential amino acids and 1.0 mmol/L of sodium pyruvate. The EOMA cells were grown in modified Eagle's medium (Cellgro) supplemented with 2 mmol/L of L-glutamine and Earle salt solution with 1.5 g/L of sodium bicarbonate and 20% heat-inactivated fetal bovine serum (Cellgro FBS).

To grow and propagate the tumors in mice, 2 × 10⁶ cells of each tumor cell line were implanted bilaterally into the gluteal region in 16 athymic female nude mice that weighed 25–30 g. A total of 32 tumors—eight tumors per tumor model—were implanted. The animals were examined with MR imaging when the tumors had grown to a diameter of 5–7 mm. The mean time between tumor implantation and MR imaging was 16 days for 9L, 13 days for HT1080, 21 days for DU4475, and 10 days for EOMA tumors. At the end of the MR imaging experiments, the animals were sacrificed by means of ketamine and xylazine overdose. All animal studies were approved by the institutional animal care committee at Massachusetts General Hospital.

MR Image Acquisition and Processing

All MR imaging studies were carried out by using a 1.5-T clinical MR imaging system (Signa; GE Medical Systems, Milwaukee, Wis) and clinically available pulse sequences. All tumor-bearing mice were anesthetized by means of intraperitoneal injection of ketamine (80 mg/kg) and xylazine (12 mg/kg). Custom-made 28-g catheters were inserted into the lateral tail veins and attached to a microheparin-saline flush unit. A 3-inch surface receiver coil was used for all studies. Following a fast spoiled gradient-echo localizer sequence (34.0/2.2 [repetition time msec/echo time msec], 30° flip angle), multiple transverse images of the tumors in each animal were obtained. All MR imaging examinations consisted of a conventional gradient-echo sequence with parameters that included 3,000/20, a 90° flip angle, a 128 × 128 matrix, and

two signals acquired. The field of view was set at 12 × 6 cm, and the section thickness was 2 mm. All animals were imaged before and after intravenous injection of 5 mg of the LCDIO agent, monocrySTALLINE iron oxide 46, per kilogram of body weight. In addition, at the end of each LCDIO-enhanced MR imaging examination, gadopentetate dimeglumine-enhanced (0.1 μmol/kg) (Magnevist, Berlex Laboratories, Wayne, NJ) spin-echo images (300/6) were obtained to outline the tumor.

Steady-state tumoral blood volume maps were calculated from the pre- and postcontrast LCDIO-enhanced MR images, as described in detail elsewhere (6,17). A fundamental assumption is that the change in the transverse relaxation rate ($\Delta R2^*$) relative to the preinjection baseline relaxation rate is proportional to the perfused local blood volume per unit tumor volume (V) multiplied by a function (f) of the plasma concentration of the agent (P): $\Delta R2^* = k \cdot f(P) \cdot V$.

Assuming a steady state of LCDIO distribution, the equation is revised to express a simple linear relationship between the change in the transverse relaxation rate and the perfused blood volume fraction: $\Delta R2^*(t) = k \cdot V(t)$ or $V(t) = [\Delta R2^*(t)]/k$, where $\Delta R2^*(t)$ is the change in the transverse relaxation rate of the tumor, $V(t)$ is the tumor volume, and the constant k includes the agent blood pool concentration and is therefore dose dependent.

The enhancement of transverse relaxation can thus be expressed as follows: $\Delta R2^* = [(1/T2^*_{\text{post}}) - (1/T2^*_{\text{pre}})] \approx (-1/TE) \cdot [\ln(S_{\text{post}}/S_{\text{pre}})]$, where S is the signal intensity; TE, the echo time; and $T2^*$, the transverse relaxation time. On the basis of this formula, maps depicting the change in transverse relaxation rate were calculated from all the MR images by using commercially available software (MatLab 7.0; The Mathworks, Waltham, Mass). In addition, two of the authors (C.B., M.M.) selected regions of interest that included the entire tumor and the adjacent muscle tissue on a given section (20–100 pixels) to calculate tumoral VVFs. Absolute tumoral VVFs were obtained by scaling measurements to muscle with a known VVF of 1.89% (18).

Tracer Blood Volume Determination

To independently verify the MR imaging measurements, we also obtained global tumoral blood volume measurements in the mice by performing nuclear

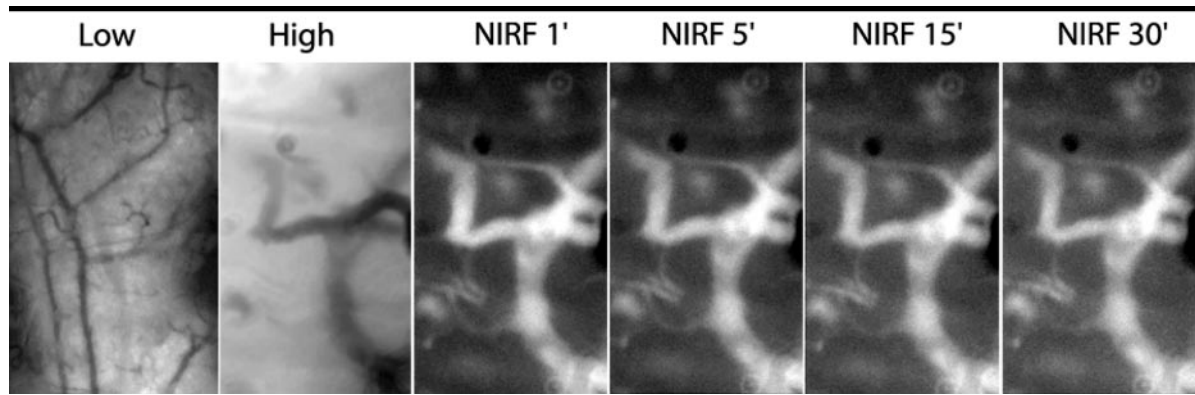


Figure 1. Intravital microscopic images enhanced with fluorescently labeled monocrystalline iron oxide 46 depict 9L tumor neovasculature. The first two images from the left are, respectively, low- (green fluorescent protein; magnification, $\times 2$) and high- (green fluorescent protein; magnification, $\times 60$) resolution images that show the vessels dark in contrast to the fluorescent tumor cells expressing green fluorescent protein. The contrast is accentuated because hemoglobin in blood vessels is an efficient absorber of fluorescent light. The third to sixth images from the left represent a time series of near-infrared fluorescent (NIRF) images obtained in the indocyanine 5.5 channel, in which the fluorescently labeled LCDIO within vessels appears bright. Note that the distribution of the intravascular probe (ie, indocyanine 5.5-labeled monocrystalline iron oxide 46) is constant during the observation time of 30 minutes; this indicates that there is no leakage. (Indocyanine 5.5-labeled monocrystalline iron oxide 46; magnification, $\times 60$.)

imaging of 10 9L, six DU4475, eight HT1080, and eight EOMA tumors. For these studies, the animals were intravenously injected with a model long-circulating intravascular probe, methoxy poly(ethylene glycol)-poly-L-lysine (PL)-diethylenetriaminepentaacetic acid (molecular weight, 500 kD), that had been labeled with technetium 99m (^{99m}Tc) (19,20). The mice were positioned so that one of the authors (M.M.) could draw select regions of interest over the tumors without measuring the blood volume of other tissues. Within 15 minutes after this intravenous administration, the animals were imaged with a modified whole-body, single-head gamma camera (M-Cam; Siemens Medical Systems, Hoffman Estates, Ill) for 1×10^6 counts. Region of interest analysis and subsequent biodistribution experiments yielded values of tumor count per gram of tissue, and, subsequently, VVF values, by means of scaling to muscle radiotracer distribution.

Intravital Microscopy

In a separate control experiment, we sought to determine whether LCDIO is truly intravascular within tumor beds during the time of normal MR image acquisition—that is, within 30 minutes after intravenous administration. For these studies, we used intravital microscopy and fluorescently (indocyanine 5.5; Amersham Biosciences, Piscataway, NJ) labeled monocrystalline iron oxide 46. For these studies, 10^6 9L tumor cells enhanced with green fluorescent protein

were injected into the ear pinna of three nu/nu mice bred at Massachusetts General Hospital. Ten days later, when the tumors had reached a size of approximately 40 mm^3 , the mice were anesthetized. Subsequently, indocyanine 5.5-labeled monocrystalline iron oxide 46 (5 mg of iron per kilogram of body weight) was injected into the lateral tail vein. The ear pinna was fixed on a microscope glass slide and observed at epifluorescent microscopy with use of different filters and magnifications ($\times 2$ – $\times 60$). Microscopic images were obtained in the green fluorescent protein (vessels appear dark on a green fluorescent protein fluorescent tumor background) and indocyanine 5.5 (vessels appear bright on a dark background) channels for up to 30 minutes after intravenous injection of the fluorescently labeled LCDIO preparation.

Histologic Microvessel Density Measurements

Microvessel density counting at histologic analysis, a much used reference standard in angiogenesis studies, was performed in all animals (21). For these measurements, the tumors were excised, snap frozen, cut into $8\text{-}\mu\text{m}$ sections, and stained for CD31. To identify vessels unequivocally, the sections were incubated with a primary anti-CD31 antibody (Santa Cruz Biotechnology, Santa Cruz, Calif) and revealed with an alkaline phosphatase-labeled secondary antibody (Sigma, St Louis, Mo). After inactivation of the endogenous alkaline phosphatase by means

of heating (65°C for 30 minutes), specific alkaline phosphatase activity was visualized by using NBT/BCIP substrate (Boehringer-Mannheim, Indianapolis, Ind). The sections were counterstained with nuclear fast red. Control sections were processed identically, with the exception of omitting the incubation with the primary antibody. Microvessel density counting was performed independently by two investigators (C.B., M.M.).

Western Blotting for Vascular Endothelial Growth Factor Measurements

Vascular endothelial growth factor (VEGF) is one of the major angiogenesis-promoting factors, and measurements of this factor have served as surrogate markers of vascularity. For these reasons, one of the authors (M.M.) also determined the VEGF levels of the different tumor cell lines. Tumor cell lysates were centrifuged for 10 minutes at 16,000 rpm. The protein content of the samples was determined by using a bicinchoninic acid assay (Pierce, Rockford, Ill). Equal amounts of protein were applied to a 12% sodium dodecyl sulfate-polyacrylamide electrophoresis gel. The proteins were separated for 50 minutes at 120 V and then blotted onto a polyvinylidene fluoride membrane (Hybond C; Amersham, Piscataway, NJ). After blocking, the membranes were incubated with a primary anti-VEGF antibody (Santa Cruz Biotechnology) and then incubated with a biotinylated secondary antibody (Vector Laboratories, Burlingame,

Calif). Binding of the antibodies was revealed by means of an alkaline phosphatase conjugate by using NBT/BCIP as a substrate. Levels of VEGF were determined by scaling the intensity of bands to known standards.

Statistical Analysis

Data are presented as means \pm standard errors of the means. Statistically significant differences between groups were determined by performing one-way analysis of variance. CIs were corrected for multiple comparisons; a *P* value of $\leq .025$ was considered to indicate a significant difference. To compare the VVFs measured at MR imaging with those measured by using radiotracer nuclear imaging, we chose the two-tailed Student *t* test. For this analysis, a *P* value of $< .05$ was considered to indicate a significant difference.

RESULTS

Intravital microscopy was initially performed to determine whether monocrySTALLINE iron oxide 46 truly had intravascular distribution in tumor microenvironments. As can be seen from Figure 1, indocyanine-labeled monocrySTALLINE iron oxide 46 selectively enhanced the tumor vascularity without any substantial leakage into the tumor interstitium during the time of observation (30 minutes). Image analysis revealed the following mean signal intensities of the tumor microvessels: 250 ± 3 at 1 minute, 250 ± 2 at 5 minutes, 248 ± 3 at 15 minutes, and 246 ± 3 at 30 minutes.

Next, we analyzed the chosen tumor models by determining microvessel counts and VEGF levels (Table). Mean VEGF levels were lowest for 9L tumors (1.8 ng/mg of protein ± 0.5), followed by DU4475 (2.3 ng/mg of protein ± 0.5), HT1080 (5.5 ng/mg of protein ± 1.9), and EOMA (7.7 ng/mg of protein ± 1.3) tumors. There were also significant ($P < .025$) differences in microvessel density count among the different tumor models (Table). Although there was typically a scattered microvessel distribution within the 9L and DU4475 tumors, there was a higher density of microvessel clusters throughout the entire tissue of HT1080 fibrosarcomas (Fig 2). The EOMA tumors had a more chaotic histologic pattern of vascularization that consisted of areas of enlarged, partially thrombosed vessels encompassed by fibrous septa filled with microvessels.

In a subsequent set of experiments, we determined the global tumoral VVF by

Summary of Experimental Measurements

| Tumor Cell Line | Cancer Type | Radiotracer VVF (%) | MR Imaging VVF (%) | MVD (counts per field)* | VEGF (ng/mg protein) |
|-----------------|---------------|----------------------------------|------------------------------------|-----------------------------------|---------------------------|
| 9L | Glioma | $2.0 \pm 0.3^{\ddagger\ddagger}$ | $2.07 \pm 0.34^{\ddagger\ddagger}$ | $43.6 \pm 3.3^{\ddagger\ddagger}$ | $1.8 \pm 0.5^{\ddagger}$ |
| DU4475 | Breast cancer | $3.0 \pm 0.2^{\ddagger}$ | $3.06 \pm 0.43^{\ddagger}$ | $39.3 \pm 2.3^{\ddagger\ddagger}$ | $2.3 \pm 0.5^{\ddagger}$ |
| HT1080 | Fibrosarcoma | $5.2 \pm 0.2^{\S}$ | $5.54 \pm 0.82^{\S}$ | $81.4 \pm 5.8^{\S\parallel}$ | 5.5 ± 1.9 |
| EOMA | Angiosarcoma | $6.1 \pm 1.2^{\parallel}$ | $6.64 \pm 0.94^{\parallel}$ | $150 \pm 13^{\S\parallel}$ | $7.7 \pm 1.3^{\parallel}$ |

Note.—All data are means \pm standard errors of the mean. The VVF measurements obtained with MR imaging were almost identical to those obtained with nuclear imaging with a radiotracer, the reference standard for comparison with MR imaging measurements.

* MVD = microvessel density.

\ddagger Value significantly different from corresponding value for HT1080 tumors ($P < .025$).

$\ddagger\ddagger$ Value significantly different from corresponding value for EOMA tumors ($P < .025$).

\S Value significantly different from corresponding value for 9L tumors ($P < .025$).

\parallel Value significantly different from corresponding value for DU4475 tumors ($P < .025$).

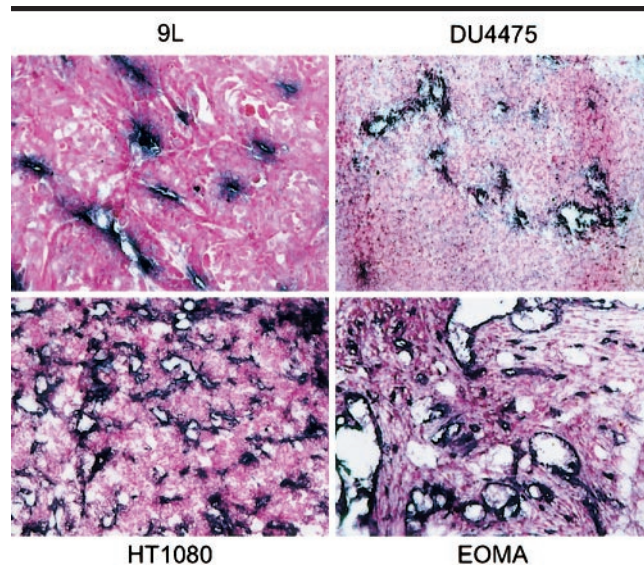


Figure 2. CD31 immunohistochemical analysis of the four experimental tumor models. Hotbeds of tumoral microvessels are stained in blue (CD31) against a red tumoral background. The microvessels in the different tumor models have different densities and morphologic appearances. (Nuclear fast red counterstain; magnification, $\times 20$.)

using a validated ^{99m}Tc marker of intravascular volume, methoxy poly(ethylene glycol)-poly-L-lysine (PL)-diethylenetriamine-pentaacetic acid (19,22). Our purpose for using this agent was to validate subsequent global MR imaging measurements, with the latter measurements being performed at much higher spatial resolutions. The VVF was lowest for 9L tumors ($2.0\% \pm 0.3$) and highest for EOMA tumors ($6.1\% \pm 1.2$) (Table). The DU4475 and HT1080 tumors had intermediate VVF values.

All tumors had similar signal intensities at T1- and T2-weighted MR imaging and were clearly demarcated from the surrounding tissues. The bilateral tumors typically had a similar overall volume; however, section-to-section variations existed

owing to slight differences in tumor implantation location (Fig 3). The global tumoral VVFs obtained in all animals are summarized in the Table. There was no statistically significant difference in global VVF values between the MR imaging and nuclear imaging (ie, radiotracer) measurements.

High-resolution VVF tumor maps for each animal imaged (Fig 3) also were obtained. Tumoral "hot spots" (ie, areas of high vascularity) usually were seen at the periphery of the tumors, similar to the highly vascular areas that had been observed at anti-CD31 immunohistochemistry. We found it interesting that the VVF in matched tumors varied widely among the different image sections and between the left and right tumors (Fig 4). This hetero-

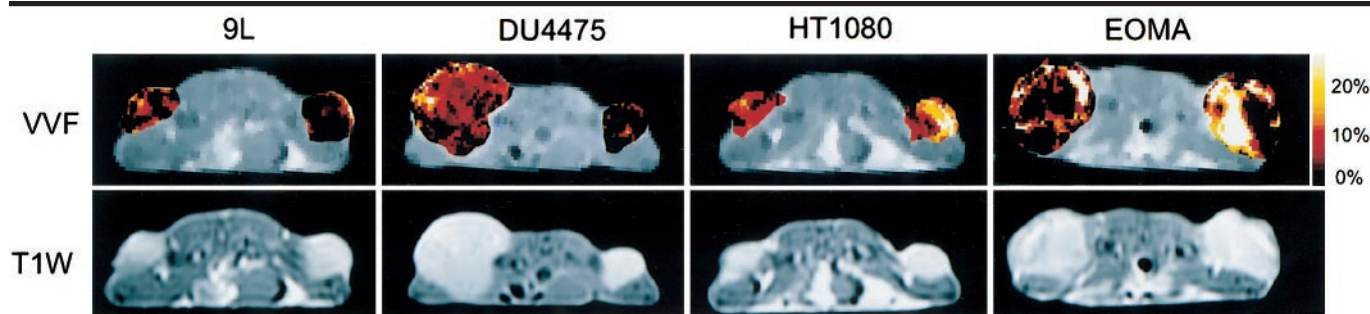


Figure 3. MR images of the four experimental tumor models. Top row: Color-coded VVF tumoral vascularity maps are superimposed onto the tumors and derived from pre- and postcontrast T2*-weighted MR imaging sequences. VVF values are from 0% to 30%. Note the heterogeneity of VVF among the tumor models. Bottom row: The different tumors are outlined on postcontrast T1-weighted spin-echo MR images (300/6).

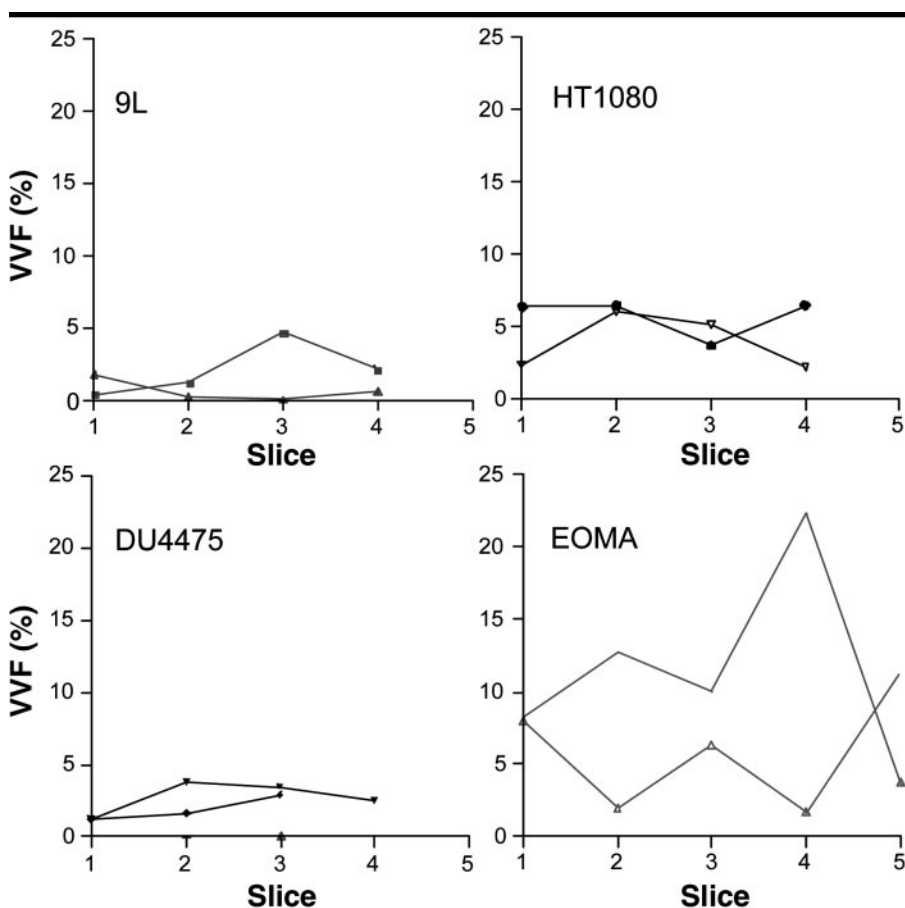


Figure 4. Graphs illustrate heterogeneity among image section–selected VVFs of different tumor models. For each model, left and right tumors within the same animal are plotted along image sections of the entire tumor. Note the considerable heterogeneity among measurements between the left and right tumors and among the different image sections of ipsilateral tumors. These changes were most dramatic in the EOMA tumors.

generality was the main rationale for performing MR imaging at high resolutions, because antiangiogenic agents may be most effective in such hot spot areas.

DISCUSSION

The results of this study confirm the unique vascular distribution of the model

LCDIO preparation used in this investigation, monocrySTALLINE iron oxide 46. We were able to achieve a truly intravascular distribution of the agent in tumor microvessels. The results of these intravital microscopic studies formed the basis for subsequent validation and MR imaging experiments. Furthermore, our study results demonstrate a close correla-

tion between overall tumoral VVF values measured at planar radiotracer scintigraphy and those measured at MR imaging. Although radiotracer VVF values could be obtained only as global measurements (small tumor size), MR imaging VVF measurements allowed serial sectioning and relatively high-resolution imaging of the vascular heterogeneity within tumors. Such angiogenic mapping is potentially valuable, because it will allow more careful analysis of intratumoral changes during antiangiogenic treatments.

Nanoparticle-based iron oxides represent one of the few classes of contrast agents with a large hydrodynamic diameter (20–50 nm) and that have been developed for clinical imaging. LCDIOs are still small enough to circulate freely in the plasma, however, even in certain vascular beds where large cells and ultrasonographic bubbles are excluded (because they have large diameters, of several micrometers). Another important factor was the development of nanoparticles with extended blood half-lives (ie, no short clearance), which has enabled MR imaging measurements to be performed in steady state.

The initial development of LCDIOs began in the late 1980s with the observation that large dextran-coated iron oxide colloids contained a fraction of small particles, which were initially termed *ultra-small superparamagnetic iron oxides* and had a long blood half-life—that is, of hours rather than minutes (14,23). Subsequent efforts to directly synthesize such small iron oxides at a higher yield were undertaken.

The structure and biologic properties of two LCDIOs synthesized with different methods, monocrySTALLINE iron oxide (24,25) and ferumoxtran (Combidex; Advanced Magnetics, Cambridge, Mass), were initially developed independently (26,27). LCDIO (monocrySTALLINE iron oxide or

ferumoxstran) consists of 4–6-nm cores of iron oxide that are covered with a layer of T-10 dextran that is approximately 10–20 nm thick; this yields an overall volume (volume weighted) of aqueous solution of 20–50 nm, depending on the preparation. Both of these LCDIOs have a blood half-life of longer than 11 hours in mice, and they have similar biodistributions. On the basis of vascular enhancement at T1-weighted MR imaging, the blood half-life of Combidex in humans is longer than 24 hours. Phase 3 clinical testing of Combidex in the United States has been completed, and this agent is commercially available in Europe. As such, this agent could be used for angiogenesis studies in patients who are undergoing antiangiogenic therapy.

Our rationale for choosing LCDIO as the contrast agent for tumoral blood volume measurements is based primarily on four observations: (a) LCDIOs have long circulation times, which allow steady-state imaging (to image multiple tumors or perform additional MR measurements), (b) the sensitivity of T2-type agents for depiction of subtle changes in blood volume should greatly exceed that of the T1-based agents (10), (c) LCDIOs are long-circulating MR imaging contrast agents that do not readily extravasate into the tumor interstitium during imaging, and (d) LCDIOs are being developed for clinical use.

Although LCDIOs have been used extensively for mapping cerebral blood volumes in task activation functional MR imaging studies (10), the use of these agents for measuring tumoral blood volumes has been less explored, and this was our rationale in performing this study. A fundamental assumption in such measurements, which is supported by detailed numeric simulations, is that the change in transverse relaxation rate relative to the baseline transverse relaxation rate before contrast agent injection is proportional to the local blood volume fraction (see Materials and Methods). Similar techniques have been used in preliminary feasibility studies in patients (28).

The results of this study confirm the hypothesis that LCDIOs can be used to measure regional tumoral VVFs at steady-state MR imaging and to map the heterogeneity of VVFs among different tumors. As shown in the Table, the MR imaging measurements seem to be reasonably accurate compared with the other surrogate markers of angiogenesis, the nuclear (ie, radiotracer) measurements of global VVF in particular. MR imaging, however, was capable of yielding high-resolution maps of VVF

distribution (Figs 3, 4), which may be particularly important in estimating the effectiveness of antiangiogenic agents, especially when they have heterogeneous effects.

Several differences between steady-state LCDIO-enhanced MR imaging and dynamic fast gadopentetate dimeglumine-enhanced MR imaging examinations of tumor vasculature are worth mentioning. First, LCDIOs represent a class of truly intravascular markers (with constant concentrations maintained during imaging) that allow steady-state imaging—that is, multiple tumors or metastases can be surveyed with a single injection of the agent. In contrast, gadopentetate dimeglumine-derived measurements are dependent on very fast MR imaging (ie, echo planar or fast gradient-echo imaging) over the same section for construction of time-activity curves that can then be used to mathematically derive parameters such as capillary permeability or surface area, blood flow, and, potentially, blood volume. One observation gleaned from intravital microscopic studies, however, is that there is marked variability in the intratumoral behavior of small molecules such as those of gadopentetate dimeglumine: Although some areas of the tumor exhibit first-pass leakage (with extraction fractions of up to 50%), other areas may exhibit much lower extractions. Predicting this behavior (as well as other parameters such as water exchange rates) mathematically may be difficult.

Finally, the various imaging methods have different sensitivities in the measurement of different physiologic parameters: Depending on the mechanism of action of a given angiogenesis inhibitor (eg, anti-VEGF action, antiendothelial action, and matrix-metalloproteinase inhibition), different approaches may be more sensitive than others. Results of intravital microscopic studies indicate that the functional tumoral VVF (ie, the perfused portion of blood within a tumor) represents a sensitive overall parameter of tumor angiogenesis.

Practical application: The described technique and its validation by means of MR imaging with a truly intravascular MR imaging radiotracer have considerable clinical applications in the measurement of tumor angiogenesis in vivo. Whether LCDIO-enhanced MR imaging is used to measure the effects of antiangiogenic agents in clinical trials or to determine the degree of vascularity in native tumors, the simplicity and validity of this examination are important aspects. Because similar agents are commercially

available in Europe and will soon be available in the United States, they can be readily used in clinical trials. To make available a noninvasive method of imaging tumor angiogenesis at high spatial resolutions and repeatedly within the same patients has been the goal of much angiogenesis imaging research.

References

1. Browder T, Butterfield CE, Kraling BM, et al. Antiangiogenic scheduling of chemotherapy improves efficacy against experimental drug-resistant cancer. *Cancer Res* 2000; 60:1878–1886.
2. Folkman J. Angiogenesis and angiogenesis inhibition: an overview. *EXS* 1997; 79: 1–8.
3. Folkman J. Tumor angiogenesis and tissue factor. *Nat Med* 1996; 2:167–168.
4. Carmeliet P, Jain RK. Angiogenesis in cancer and other diseases. *Nature* 2000; 407: 249–257.
5. Kerbel RS. Clinical trials of antiangiogenic drugs: opportunities, problems, and assessment of initial results. *J Clin Oncol* 2001; 19(18 suppl):455–515.
6. Dennie J, Mandeville JB, Boxerman JL, Packard SD, Rosen BR, Weisskoff RM. NMR imaging of changes in vascular morphology due to tumor angiogenesis. *Magn Reson Med* 1998; 40:793–799.
7. Taylor JS, Tofts PS, Port R, et al. MR imaging of tumor microcirculation: promise for the new millennium. *J Magn Reson Imaging* 1999; 10:903–907.
8. Hawighorst H, Weikel W, Knapstein PG, et al. Angiogenic activity of cervical carcinoma: assessment by functional magnetic resonance imaging-based parameters and a histomorphological approach in correlation with disease outcome. *Clin Cancer Res* 1998; 4:2305–2312.
9. Hawighorst H, Knapstein PG, Knopp MV, et al. Uterine cervical carcinoma: comparison of standard and pharmacokinetic analysis of time-intensity curves for assessment of tumor angiogenesis and patient survival. *Cancer Res* 1998; 58:3598–3602.
10. Mandeville JB, Marota JJ, Kosofsky BE, et al. Dynamic functional imaging of relative cerebral blood volume during rat forepaw stimulation. *Magn Reson Med* 1998; 39:615–624.
11. Brasch R, Pham C, Shames D, et al. Assessing tumor angiogenesis using macromolecular MR imaging contrast media. *J Magn Reson Imaging* 1997; 7:68–74.
12. Weissleder R, Bogdanov A Jr, Tung CH, Weinmann HJ. Size optimization of synthetic graft copolymers for in vivo angiogenesis imaging. *Bioconjug Chem* 2001; 12:213–219.
13. Weissleder R, Bogdanov A, Papisov M. Long-circulating iron oxides for MR imaging. In: *Advanced drug delivery reviews*. Boca Raton, Fla: CRC, 1995; 321–334.
14. Weissleder R, Elizondo G, Wittenberg J, Rabito CA, Bengele HH, Josephson L. Ultrasmall superparamagnetic iron oxide: characterization of a new class of contrast agents for MR imaging. *Radiology* 1990; 175:489–493.
15. Jung C, Weissleder R, Josephson L. Phys-

- ical properties of MION-46 and AMI-227 (abstr). In: Proceedings of the Fourth Meeting of the International Society for Magnetic Resonance in Medicine. Berkeley, Calif: International Society for Magnetic Resonance in Medicine, 1996; 1681.
16. Obeso J, Weber J, Auerbach R. A hemoendothelioma-derived cell line: its use as a model for the study of endothelial cell biology. *Lab Invest* 1990; 63:259–269.
 17. Boxerman JL, Hamberg LM, Rosen BR, Weisskoff RM. MR contrast due to intravascular magnetic susceptibility perturbations. *Magn Reson Med* 1995; 34:555–566.
 18. Zhu H, Melder RJ, Baxter LT, Jain RK. Physiologically based kinetic model of effector cell biodistribution in mammals: implications for adoptive immunotherapy. *Cancer Res* 1996; 56:3771–3781.
 19. Callahan R. Validation of plasma volume determinations in the rat using an In-111 labeled polymer and I-125 labeled human serum albumin (abstr). *J Nucl Med* 1995; 157P.
 20. Callahan RJ, Bogdanov A Jr, Fischman AJ, Brady TJ, Weissleder R. Preclinical evaluation and phase I clinical trial of a ^{99m}Tc-labeled synthetic polymer used in blood pool imaging. *AJR Am J Roentgenol* 1998; 171:137–143.
 21. Weidner N, Folkman J, Pozza F, et al. Tumor angiogenesis: a new significant and independent prognostic indicator in early-stage breast carcinoma. *J Natl Cancer Inst* 1992; 84:1875–1887.
 22. Bogdanov AA, Lewin M, Weissleder R. Approaches and agents for imaging the vascular system. *Adv Drug Deliv Rev* 1999; 37:279–293.
 23. Weissleder R, Elizondo G, Wittenberg J, Lee AS, Josephson L, Brady TJ. Ultrasmall superparamagnetic iron oxide: an intravenous contrast agent for assessing lymph nodes with MR imaging. *Radiology* 1990; 175:494–498.
 24. Weissleder R, Lee AS, Khaw BA, Shen T, Brady TJ. Antimyosin-labeled monocry-
 25. talline iron oxide allows detection of myocardial infarct: MR antibody imaging. *Radiology* 1992; 182:381–385.
 26. Shen T, Weissleder R, Papisov M, Bogdanov A, Brady T. Monocrystalline iron oxide nanocompounds (MION): physicochemical properties. *Magn Reson Med* 1993; 29:599–604.
 27. Jung C. Surface properties of superparamagnetic iron oxide MR contrast agents: ferumoxides, ferumoxtran, ferumoxsil. *Magn Reson Imaging* 1995; 13:675–691.
 28. Jung C, Jacobs P. Physical and chemical properties of superparamagnetic iron oxide MR contrast agents: ferumoxides, ferumoxtran, ferumoxsil. *Magn Reson Imaging* 1995; 13:661–674.
 29. Enochs WS, Harsh G, Hochberg F, Weissleder R. Improved delineation of human brain tumors on MR images using a long-circulating, superparamagnetic iron oxide agent. *J Magn Reson Imaging* 1999; 9:228–232.